Temporal Contour Integration Deficits in Children With Amblyopia

Yan-Ru Chen,[1] Shu-Qi Jiang,[1] Xiang-Yun Liu,[2] and Jun-Yun Zhang[1]

[1]School of Psychological and Cognitive Sciences, and Beijing Key Laboratory of Behavior and Mental Health, Peking University, Beijing, China
[2]Department of Ophthalmology, Tengzhou Central People's Hospital, Tengzhou, Shandong Province, China

Correspondences: Jun-Yun Zhang, School of Psychological and Cognitive Sciences, Peking University, Beijing 100871, China; zhangjunyun@pku.edu.cn.
Xiang-Yun Liu, Department of Ophthalmology, Tengzhou Central People's Hospital, Tengzhou, Shandong Province 277599, China; zhuanghqqq@126.com.

YRC and SQJ contributed equally to this work and should be considered co-first authors.

Received: August 31, 2024
Accepted: March 19, 2025
Published: April 11, 2025

Citation: Chen Y-R, Jiang S-Q, Liu X-Y, Zhang J-Y. Temporal contour integration deficits in children with amblyopia. *Invest Ophthalmol Vis Sci.* 2025;66(4):27. https://doi.org/10.1167/iovs.66.4.27

Purpose. Contour integration, the process of combining local visual fragments into coherent paths or shapes, is essential for visual perception. Although prior research on amblyopia has focused primarily on spatial domain deficits in contour integration, this study investigates how amblyopia affects contour integration over time and examines the relationship between temporal contour integration deficits and visual functions.

Methods. Nineteen amblyopic children (mean age, 10.9 ± 2.4 years; 17 anisometropic, 2 anisometropic/strabismic mixed) and 26 visually normal children (mean age, 10.5 ± 1.8 years) participated in this study. Temporal contour integration was assessed by measuring the accuracy of detecting tilted contour paths, formed by collinear Gabor elements with similar orientations, under slit-viewing conditions. Performance was evaluated for amblyopic eyes (AEs) and fellow eyes (FEs) at two spatial frequencies (1.5 cpd and 3 cpd). The slit width, orientation jitter of contour elements, and stimulus movement speed were systematically varied across separate runs. Visual acuity and Randot stereoacuity were assessed before testing.

Results. AEs exhibited significant deficits in temporal contour processing compared with FEs. Specifically, AEs required larger slit widths to achieve performance levels comparable to FEs, with more severe amblyopia (i.e., worse AE visual acuity) necessitating even larger slit widths for temporal contour integration. Temporal contour integration deficits in AEs were most pronounced under conditions of complete Gabor collinearity or moderate stimulus movement speeds (6.4°/s). No significant differences were observed between FEs and control eyes. Notably, the temporal contour integration ability between the two eyes quantified as the AE/FE ratio of slit width thresholds showed no correlation with interocular acuity differences, stereoacuity, or spatial contour integration deficits.

Conclusions. Amblyopic children demonstrate significant deficits in temporal contour integration in AEs, which seem to be independent of spatial contour integration deficits. The severity of these temporal deficits increases with worse AE visual acuity. These findings suggest that amblyopia is associated with temporal deficits in visual integration, in addition to the well-documented spatial deficits, highlighting the need for a more comprehensive understanding of amblyopic visual processing.

Keywords: amblyopia, anisometropia, contour integration, temporal integration, slit viewing

Amblyopia is a developmental visual disorder typically caused by strabismus, anisometropia, or selective deprivation of vision during early childhood. It is attributed to complex neural deficits in both the striate and extrastriate cortices,[1] resulting in significant unilateral visual loss, particularly in children. Amblyopia is associated with deficits in multiple spatial visual functions, including reduced visual acuity,[2] impaired contrast sensitivity,[3,4] diminished stereopsis,[5,6] and compromised global shape perception.[7,8] Although most research has focused on visual function deficits in the amblyopic eye (AE), emerging evidence suggests that the fellow eye (FE) may also exhibit visual function impairments compared with normal control eyes.[9,10]

Amblyopia not only impairs spatial processing, but also affects temporal processing. These temporal deficits include reduced temporal contrast sensitivity,[11,12] abnormal motion-defined form perception,[13,14] impaired global motion perception,[13,15,16] temporal instability,[17,18] and deficits in temporal synchrony.[19,20] Research has shown that temporal deficits are not confined only to AEs, but are also present in FEs, albeit to a lesser degree.[14–16,19] For example, children with unilateral amblyopia exhibit motion processing impairments in their FEs, even when the measures of visual acuity are within the normal range.[21,22] Although some studies have reported correlations between temporal deficits and spatial deficits in amblyopia,[17,18,23,24] others suggest that certain temporal deficits exist independent of spatial vision impair-

ments.[16,19,20,25,26] For instance, Kiorpes et al.[26] demonstrated in amblyopic monkeys that motion sensitivity losses were uncorrelated with spatial contrast sensitivity losses.

Contour integration, the process of integrating physically discontinuous visual fragments into a perceived contour, is a fundamental aspect of higher-level visual processing.[27] In a seminal study, Field et al.[28] used a snake-like contour path composed of Gabor elements embedded in a noise background to demonstrate the critical role of continuity among neighboring elements in contour integration. Both spatial and temporal parameters of contour integration are frequently examined through local mechanisms, such as collinear facilitation, where the contrast sensitivity to a low-contrast Gabor target is enhanced by spatially separated collinear flankers.[29–31] These findings suggest that local interactions between neighboring elements underlie contour integration. Similar to collinear facilitation, contour integration is thought to involve excitatory horizontal connections between cells with similar orientation preferences within the primary visual cortex (V1),[28,32–36] supported by neurophysiological evidence.[37–43] Neuroimaging studies have further implicated both striate and extrastriate cortices, including V2, V4v, and the lateral occipital complex, contributing to contour integration.[44,45] Recent research indicates that contour integration involves both bottom-up and top-down (reentrant) processes.[46–49]

Amblyopic individuals exhibit abnormal performance in both lateral interactions[50–54] and spatial contour integration.[55–61] For example, Polat et al.[50] found that collinear flankers facilitated the detection of low-contrast Gabor targets in control subjects, whereas this facilitatory effect was absent or even reversed in individuals with strabismic and/or anisometropic amblyopia. Similarly, studies investigating contour detection in noise revealed that contour visibility in strabismic amblyopia was degraded by random orientation offset from the contour path, confirming the critical role of collinearity in contour integration.[55,61] Interestingly, Hess and Demanins[62] reported no contour integration deficits in most adults with anisometropic amblyopia using a contour detection task. In contrast, Levi et al.[57] identified mild but genuine contour integration deficits in adults with anisometropic amblyopia using a contour discrimination test. Recently, we demonstrated that children treated for anisometropic amblyopia still exhibited contour integration deficits, particularly at higher spatial frequencies, even after compensating for low-level deficits such as reduced contrast sensitivity and degraded shape perception in AEs.[60] These findings suggest that contour integration deficits in amblyopia may arise from impairments in both low-level and high-level visual processing.

Visual systems can integrate information over time to perceive an object's shape, even when it moves behind a narrow slit.[63] Although most studies have focused on spatial contour integration, Kuai et al.[64] were the first to investigate the mechanisms of temporal contour integration systematically. They developed a contour integration task under slit viewing conditions, in which stimuli moved horizontally behind a vertical slit, allowing only a small portion of the stimuli to be visible at any given time. They found that young adults with normal visual acuity demonstrated robust contour detection, even when the slit permitted only one viewable contour element. This finding suggests that, unlike spatial contour integration, horizontal connections in V1 may not be necessary for temporal contour integration.[32,65] Using functional magnetic resonance imaging, Kuai et al.[64] further demonstrated that temporal contour processing primarily involved higher dorsal visual areas (e.g., V3B and MT) and higher ventral visual areas lateral occipital complex, but not early visual areas (e.g., V1 and V2). These findings suggest that the neural mechanisms underlying the Gestalt rule of continuity in contour integration are at least dissociated partially between spatial and temporal domains, with temporal contour integration relying more heavily on higher-order visual regions.

Despite extensive research on spatial contour integration in amblyopia, the impact of amblyopia on temporal contour integration remains poorly understood, particularly in children. Furthermore, it is unclear whether performance differences exist between the FEs and normal control eyes in temporal contour integration. In this study, we adopted the slit-viewing task developed by Kuai et al.[64] to examine temporal contour integration in 19 amblyopic children. We compared the performance of detecting tilted contour paths composed of collinear Gabor elements under slit viewing conditions among the AEs, FEs, and normal control eyes. Additionally, we investigated the influence of Gabor orientation collinearity and stimulus movement speed on temporal contour integration in amblyopic and normal vision children. We also explored the relationships between temporal contour integration deficits and other visual functions, including monocular visual acuity, binocular stereoacuity, and spatial contour integration.

Methods

Participants

Amblyopia was defined as a best-corrected visual acuity in the AE of less than 0.1 logMAR and an interocular acuity difference of no less than 0.1 logMAR.[66] This clinical definition of amblyopia was adopted as part of our inclusion and exclusion criteria. Anisometropia was defined as a difference of 1.00 diopters (D) or more in the myopic, hyperopic, or astigmatic refractive error between the observer's two eyes. Strabismus was defined as a 5 to 50 prism diopter angular deviation between two eyes at either near or far viewing distances.

Nineteen amblyopic children aged 8.0 to 16.5 years (13 boys and 6 girls; mean age, 10.9 ± 2.4 years; 17 anisometropic and 2 anisometropic/strabismic mixed) met the inclusion criteria, and their data were included in the analysis (detailed clinical information is provided in Table). Three additional children participated in the study but were excluded from the analysis because they did not meet the inclusion criteria: one was a successfully treated patient with refractive amblyopia (<0.1 logMAR best-corrected visual acuity in the weak eye after treatment), and the other two were strabismic patients with 0.1 logMAR best-corrected visual acuity in the weak eye and a 0.1 logMAR interocular acuity difference. All participants underwent ophthalmological examinations and were refracted by a registered optometrist before testing. Participants who had been prescribed refractive correction were required to wear their glasses throughout the experiment.

Twenty-six children aged 8 to 13 years (12 boys and 14 girls; mean age, 10.5 ± 1.8 years) with normal or corrected-to-normal visual acuity and normal stereoacuity (mean, 33.2 ± 11.7 arcsec) participated as control groups ($n = 11$, $n = 10$, and $n = 7$ for experiments 1, 2, and 3, respectively; 1 observer participated in all 3 experiments).

Investigative Ophthalmology & Visual Science

Table. Characteristics of Amblyopic Children

Observer	Age (Y)	Sex	Diagnosis	Strabismus	Eye	Refractive Correction	Best-Corrected Visual Acuity (logMAR)	Severity	Stereoacuity (Arcsec)	Past Treatment	Experiments
S1	13.0	Male	A	None	AE (R)	+3.25/−2.00 × 170	0.92	Sev	F	Glasses	1
					FE (L)	+3.00/−1.25 × 165	0.22				
S2	10.8	Female	A	None	AE (L)	+2.00	0.82	Sev	F	Corrective surgery	2
					FE (R)	+4.25	0.40				
S3	11.0	Male	A	None	AE (R)	+3.50/−1.25 × 140	0.60	Mod	70	Patching glasses	1, 2, and 3
					FE (L)	−0.25/−1.00 × 5	0.22				
S4	12.3	Female	A	None	AE (L)	+2.00	0.22	Mild	200	Patching glasses	1 and 2
					FE (R)	Plano	0				
S5	8.0	Male	S	45Δ EsoT	AE (L)	none	0.70	Sev	F	None	1, 2, and 3
					FE (R)	none	0.22				
S6	8.9	Male	A	None	AE (L)	+6.50/−1.00 × 175	0.22	Mild	F	Patching glasses	1 and 2
					FE (R)	+2.75/−0.25 × 155	0				
S7	9.9	Male	A	None	AE (R)	+7.00	0.22	Mild	40	Patching glasses	1 and 2
					FE (L)	+7.50/−1.25 × 160	0				
S8	15.8	Female	A and S	30Δ ExoT	AE (R)	+3.50	0.40	Mod	F	None	2
					FE (L)	Plano	0				
S9	16.5	Male	A	None	AE (R)	−5.75/−1.50 × 175	0.92	Sev	F	None	1
					FE (L)	−8.75	0				
S10	9.0	Male	A	None	AE (R)	+1.75/−0.75 × 160	0.30	Mod	120	Glasses	3
					FE (L)	+0.50/−1.00 × 180	0				
S11	11.1	Female	A	None	AE (L)	+4.00/−0.50 × 65	0.92	Sev	F	Glasses	1, 2, and 3
					FE (R)	Plano	0.22				
S12	8.6	Male	A	None	AE (L)	+6.50	0.40	Mod	200	Glasses	1, 2, and 3
					FE (R)	Plano	−0.08				
S13	12.9	Male	A	None	AE (R)	+3.50/−0.75 × 5	0.40	Mod	F	None	1, 2, and 3
					FE (L)	−0.50/−0.75 × 170	0				
S14	8.0	Male	A	None	AE (L)	+4.00/−0.50 × 6	0.22	Mild	200	Glasses	1 and 2
					FE (R)	Plano	0				
S15	11.9	Male	A	None	AE (R)	+6.00/−1.25 × 176	0.52	Mod	F	Patching glasses	1, 2, and 3
					FE (L)	+1.75/−0.50 × 167	0				
S16	10.0	Male	A	None	AE (L)	+4.00/−1.00 × 3	0.22	Mild	50	Patching glasses	1 and 2
					FE (R)	Plano	−0.08				
S17	8.5	Female	A	None	AE (R)	+4.50/−1.25 × 170	0.82	Sev	F	Patching glasses	1
					FE (L)	Plano	0				
S18	11.0	Male	A	None	AE (L)	+1.25/−3.75 × 180	0.22	Mild	100	Patching glasses	1 and 2
					FE (R)	−1.00	0.10				
S19	9.0	Female	A	None	AE (L)	+2.75/−1.50 × 40	0.30	Mod	25	Glasses	1, 2, and 3
					FE (R)	−1.25	0				

A, anisometropic; AE, amblyopic eye; EsoT, esotropia; ExoT, exotropia; F, failed the Randot Stereo Test; FE, fellow eye; L, left; R, right; S, strabismic.

Strabismus was diagnosed using a cover test at a distance of 33 cm.

Severity: amblyopia severity was defined based on AE logMAR acuity while wearing refractive correction. Observers were stratified into three groups: mild = mild amblyopia (0.1–0.3 logMAR); mod = moderate amblyopia (0.3 ≤ AE acuity ≤ 0.6 logMAR); sev = severe amblyopia (>0.6 logMAR).

Experiments indicates the experiment(s) in which each observer participated. Note: In Experiment 1, observer S7 was only tested under the 3 cpd condition, whereas observers S9, S13, and S14 were only tested under the 1.5 cpd condition. In Experiment 2, observer S6 was only tested under the 1.5 cpd condition.

The study adhered to the tenets of the Declaration of Helsinki and was approved by the ethics committees of Tengzhou Central People's Hospital and Peking University. Informed consent was obtained from each participant's parent or guardian after a detailed explanation of the nature and potential consequences of the study.

Apparatus and Stimuli

The stimuli were generated with MATLAB-based Psychtoolbox-3[67] and presented on a 21-inch Sony G520 CRT monitor with a display resolution of 1024 × 768 pixels and a frame rate of 75 Hz. The luminance of the monitor was linearized by an 8-bit look-up table (mean luminance, 58.2 cd/m^2). Observers viewed the displays monocularly, with the nontested eye patched. A chin-and-head rest was used to stabilize the observer's head. The experiments were conducted in a dimly lit room.

The stimuli used in this study were similar to those in Kuai et al. (2017).[64] They consisted of 256 Gabor patches (Gaussian-windowed sinusoidal gratings) presented within 256 squares of a 16 × 16 invisible grid. Each square subtended 1.650° or 0.825° at viewing distances of 0.5 or 1.0 meter, respectively. The spatial frequency of the Gabor elements was set to 1.5 and 3.0 cycles per degree (cpd) for viewing distances of 0.5 and 1.0 meter. The contrast of the Gabor elements was fixed at 90% and their phases were randomized between 0° and 315° in a step of 45°. The standard deviation of the Gabor Gaussian envelope (σ) was always equal to 0.45 times the Gabor wavelength (λ). All Gabor elements, whether part of contour or noise, were physically identical except for their phases, locations, and orientations.

A straight contour path formed by nine collinear Gabor elements was embedded in a field of noise Gabor patches (Fig. 1A, left). The stimulus images moved horizontally behind a vertical slit, either from left to right or vice versa (Figs. 1B, 1C). The center of the contour path was positioned at the stimulus center with a positional jitter within ±2.5°, and the orientation of the contour path varied between 15° to 60° or 120° to 165°. Each noise Gabor was positioned in a square with random orientations and positional jitter within

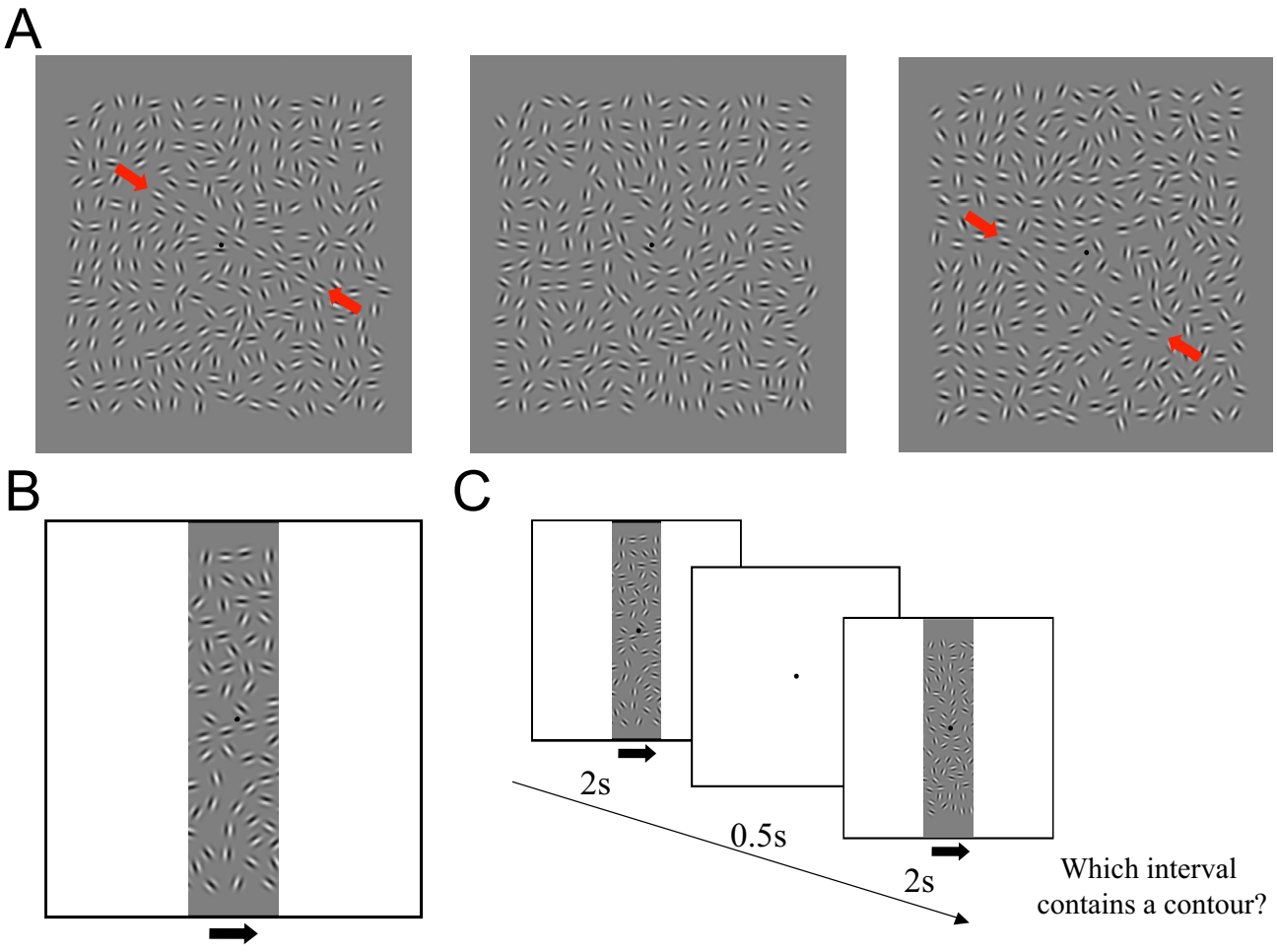

Figure 1. Stimuli used in temporal contour integration experiments. (**A**) (*Left*) A straight contour without position or orientation jitter, embedded in a field of randomly positioned Gabor patches. (*Middle*) Random Gabor patches with no contour path. (*Right*) Contour Gabor elements with orientations jittered within ±20° from the contour path orientation (stimuli used in experiment 2). *Red arrows* are included for illustrative purposes and were not present in the actual stimuli. (**B**) An example frame of stimuli moving behind a vertical slit with an AIED of 4. (**C**) Trial structure: Two stimulus images, one containing a contour and the other without, moved behind a vertical slit for 2 seconds, either left to right or right to left, separated by a 0.5-second interstimulus interval. Observers were instructed to identify the interval containing the contour. *Arrows* are shown here for clarity and were not included in the actual stimuli.

Investigative Ophthalmology & Visual Science

±0.25 square size in both horizontal and vertical directions from the grid center. To avoid density cues, the center-to-center horizontal distance between neighboring contour Gabor elements was randomized between 0.9 and 1.1 times the average interelement distance (AIED), which was equal to the size of the square. The stimulus pattern was regenerated for each trial. Within the same trial, a random stimulus image (without any contour path) was generated by randomly shuffling the positions of all Gabors in the contour stimulus image (Fig. 1A, middle).

Procedures

For amblyopic children, we measured contour detection performance for AEs and FEs separately using a two-interval forced-choice method of constant stimuli. In experiment 1, two stimulus images were presented in each trial: one image contained a contour (Fig. 1A, left) and the other image did not contain a contour (Fig. 1A, middle). The images moved behind a vertical slit of varying widths (0.4, 0.8, 1.0, 2.0, and 4.0 times the AIED) from left to right or vice versa at a speed of 6.4°/s for 2 seconds. The two intervals were separated by an interstimulus interval of 500 ms (Figs. 1B, 1C). A black fixation dot, serving as a reference point for the center of the stimulus, remained visible throughout the trial. Fixation accuracy was not explicitly controlled during the experiment. Observers were permitted to freely view the stimulus, and their responses were based on their perception of the contour. Auditory feedback was given on incorrect responses.

Five slit width conditions (0.4, 0.8, 1.0, 2.0, and 4.0 times the AIED) were tested. The observer can see only one contour element or part of it when the slit width was 0.4 AIED, parts of two neighboring contour elements for the slit width of 0.8 AIED, two neighboring contour elements at the same time for 1 AIED, and more than two neighboring contour elements at any given moment for 2 and 4 AIEDs. Each condition was tested in separate blocks, with 50 trials per block. Each condition was measured two to four times.

The spatial frequency of Gabor elements was set at 1.5 or 3.0 cpd, achieved by adjusting the viewing distance to 0.5 or 1.0 meter, respectively. To measure spatial contour integration in amblyopia, contour detection performance was assessed using a static screen (i.e., without an aperture or slit). Two static stimulus images were presented: one image contained a contour and the other image did not contain a contour. Each image was displayed for 200 ms each, separated by an interstimulus interval of 500 ms. Observers were asked to judge which interval contained a contour.

The procedures in experiments 2 and 3 were nearly identical to experiment 1, except for changes in specific stimulus parameters. In experiment 2, the orientations of individual contour Gabor elements were jittered within a range of 0°, ±10°, ±20°, ±30°, or ±45° from the contour path (Fig. 1A, right). The slit width was fixed at 1 AIED, and the speed of stimulus movement was 6.4°/s. In experiment 3, the speed of stimulus movement was varied within a range of 1.6°/s, 3.2°/s, 6.4°/s, 12.8°/s, or 25.6°/s. The slit width was fixed at 1 AIED and only 1.5 cpd Gabors were used in experiment 3.

Twenty-six visually normal children participated as the control groups and were tested in experiments 1 and 2 at 3 cpd and experiment 3 at 1.5 cpd Gabors. The contour detection performance for dominant and nondominant eyes was measured separately for the control group in experiment 1. Because the performances between the dominant and FEs in the control group had no significant difference in experiment 1 (see the detail in Results), only one eye of the observers in control groups in experiments 2 and 3 was tested, which was randomly chosen at the beginning of the test. Each block consisted of 30 trials and was repeated two to four times. The viewing distance was 0.5 or 1.0 meter when the tested spatial frequency of Gabor elements was set at 1.5 or 3.0 cpd, respectively.

Assessment of Visual Acuity and Stereoacuity

Before conducting the temporal contour integration tests, visual acuity and stereoacuity were assessed for all observers. Visual acuity was assessed with the Chinese Tumbling E Chart,[68] which has 14 lines, with the size of the optotypes ranging from 1.0 to −0.3 logMAR in 0.1-logMAR steps. Testing was performed monocularly at a distance of 5 meters from the chart, with the nontested eye occluded. Observers were required to report the orientation of the opening of the tumbling E. Visual acuity was recorded as the logMAR.

Stereoacuity was assessed using the Randot Stereo Test (Stereo Optical Co., Inc., Chicago, IL) under normal room lighting conditions. Observers wore a pair of polarizer glasses and were asked to identify which of the three circles in a line appeared to stand in front. The test included ten three-circle lines with binocular disparities ranging from 400 to 20 arcsec. Testing was conducted at a viewing distance of 40 cm. For observers who failed to identify the circle with the largest disparity (400 arcsec), stereoacuity was set to 500 arcsec for the convenience of data analysis.

Data Analysis

In experiment 1, a Weibull function was used to fit the psychometric function for each observer. The fitting was conducted using the Matlab version of the Psignifit toolbox (version 2.5.6), developed by Psignifit Wichmann lab of the University of Tübingen.[69]

To explore the factors influencing temporal contour integration in amblyopic observers, we first analyzed the effects of the AE visual acuity and stereoacuity on performance. Amblyopic observers were divided into three groups based on their AE visual acuities measured before testing: mild amblyopia (AE acuity $<$ 0.3 logMAR), moderate amblyopia (0.3 $\leq$ AE acuity $\leq$ 0.6 logMAR), and severe amblyopia (AE acuity $>$ 0.6 logMAR).[70] ANOVA revealed no significant differences in temporal contour integration among the three AE severity groups (Ps $>$ 0.05) across all three experiments. Amblyopic observers were also divided into two groups based on their stereoacuity measurements: those who failed the Randot Stereo Test (assigned 500 arcsec, no stereopsis group), and those who had measurable stereoacuity (stereopsis group). Again, ANOVA found no significant differences in temporal contour integration between the no stereopsis and stereopsis groups (Ps $>$ 0.05) across all three experiments. Given the lack of significant differences based on AE visual acuity or stereoacuity, we combined temporal contour integration data from all amblyopic children for analysis in experiments 1, 2, and 3, unless otherwise specified.

All analyses were conducted using open-source JASP software (version 16.3). A one-sample t test was used to compare AE/FE ratios of contour detection accuracy and slit width thresholds with the value of 1.0, which indicates equal performance between AEs and FEs. Paired t tests

Investigative Ophthalmology & Visual Science

or repeated-measures ANOVA were employed for within-group comparisons (e.g., AEs vs. FEs). One-way ANOVA was used to compare performance between the amblyopic group and the normal control group. Pearson's r correlation was applied to assess the potential influence of visual functions (e.g., visual acuity, stereoacuity) on temporal contour integration deficits in amblyopic children.

Results

Temporal Contour Integration in Amblyopic Children and Children With Normal Vision

In experiment 1, we investigated the temporal contour integration ability of amblyopic children using Gabor element arrays moving at a speed of 6.4°/s behind five slit widths (0.4, 0.8, 1.0, 2.0, and 4.0 times the AIED). To assess performance across different spatial scales, Gabor elements with spatial frequencies of 1.5 and 3 cpd were used, achieved by setting the viewing distance to 0.5 and 1.0 meter, respectively.

The mean accuracy of amblyopic observers is shown in Figures 2A and 2D. Contour detection accuracy increased with larger slit widths for both AE and FE. High accuracy levels (≥0.8) were achieved at a slit width of 4 times the AIED, comparable with the performance observed when no aperture or slit was present (i.e. the entire Gabor array was visible). A three-way repeated measures ANOVA, with Gabor spatial frequency (1.5 and 3 cpd), eye (AEs vs. FEs), and slit width (0.4, 0.8, 1.0, 2.0, and 4.0 times the AIED) as factors, revealed significant main effects of the eye, $F(1, 11) = 20.60$, $P < 0.001$, $\eta_p^2 = 0.65$, and slit width, $F(4, 44) = 54.04$, $P < 0.001$, $\eta_p^2 = 0.65$, indicating pronounced differences in contour detection accuracy between AEs and FEs. Notably, at the 0.4 AIED slit width, where only one Gabor element or part of it was visible at any time, AEs demonstrated accuracy significantly above chance level (0.5) for both spatial frequencies: 1.5 cpd (accuracy = 0.61 ± 0.08, $t_{14} = 5.95$, $P < 0.001$, Cohen's $d = 1.54$) and 3 cpd (accuracy = 0.61 ± 0.08, $t_{12} = 5.08$, $P < 0.001$, Cohen's $d = 1.41$, one sample t test).

To quantify interocular performance differences, we calculated the AE/FE ratio of accuracy for each slit width

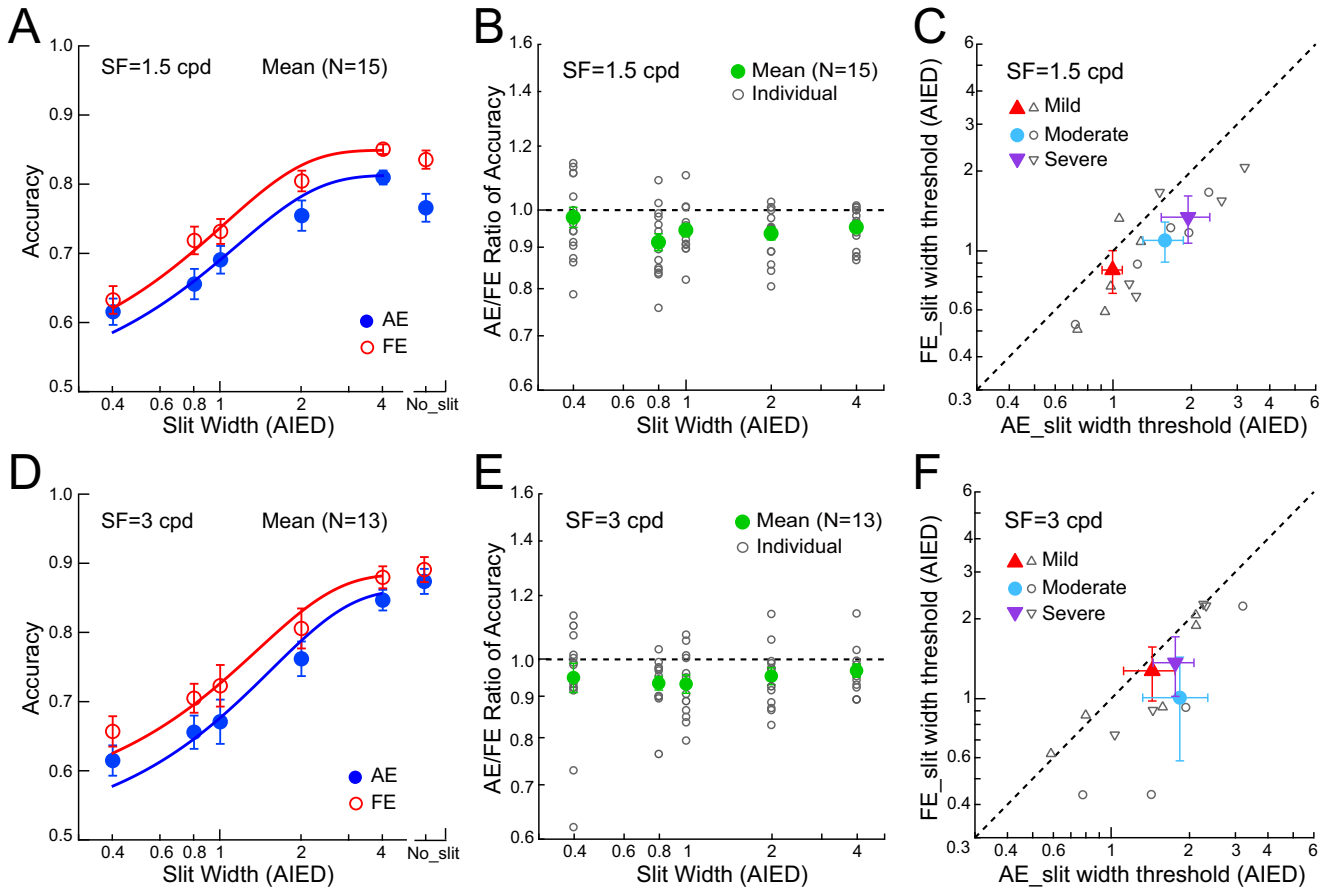

Figure 2. Temporal contour integration performance in amblyopic children. (**A** and **D**) Mean accuracy of contour detection as a function of slit width for AEs and FEs at Gabor spatial frequency of 1.5 cpd (**A**) and 3 cpd (**D**). *Smooth curves* represent Weibull function fits (1.5 cpd: $R^2 = 0.996$ for AE, $R^2 = 0.997$ for FE; 3 cpd: $R^2 = 0.997$ for AE, $R^2 = 0.996$ for FE). Dots to the right of the curve indicate accuracy under no aperture/slit conditions (i.e., the entire Gabor array was visible). (**B** and **E**) AE/FE ratio of accuracy at five slit widths for 1.5 cpd (**B**) and 3 cpd (**E**). Data points below the dashed line indicate lower accuracy in AEs compared with FEs. *Large dots*, mean thresholds; *small dots*, individual thresholds. (**C** and **F**) Slit width thresholds for AEs and FEs at 1.5 cpd (**C**) and 3 cpd (**F**). Data points below the diagonal line indicate higher thresholds in AEs compared with FEs. Symbols represent amblyopia severity: *triangles*, mild amblyopia; *circles*, moderate amblyopia; *inverted triangles*, severe amblyopia. Large symbols: mean thresholds for each group; small symbols: individual thresholds. Error bars represent ±1 SEM.

Investigative Ophthalmology & Visual Science

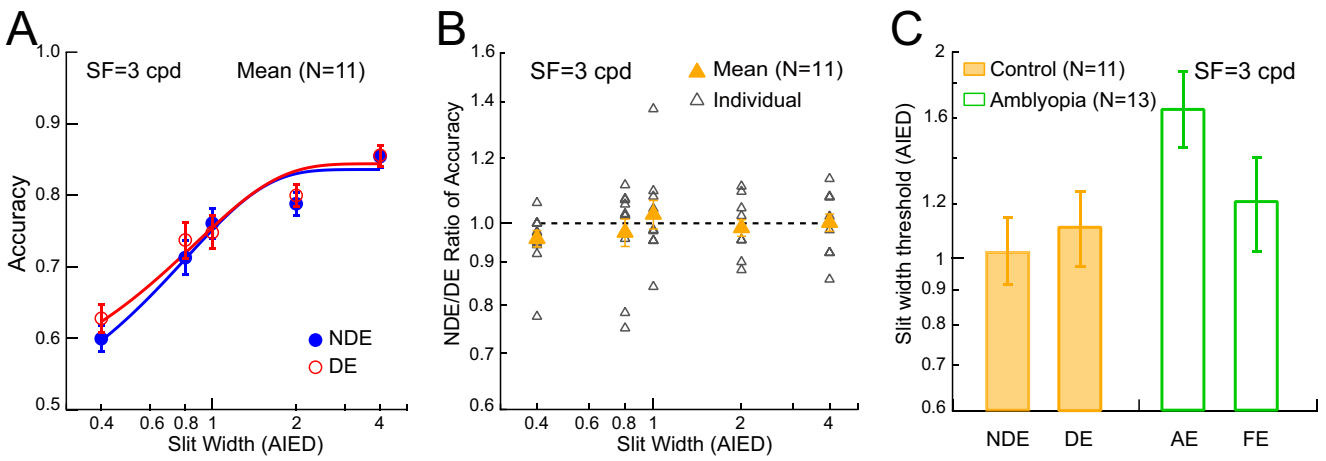

Figure 3. Temporal contour integration performance in normal controls. (**A**) Mean accuracy of contour detection as a function of the slit width for nondominant eyes (NDEs) and dominant eyes (DEs). Smooth curves represent Weibull function fits ($R^2 = 0.995$ for the nondominant eye; $R^2 = 0.996$ for the dominant eye). (**B**) The ratio of accuracy between NDEs and DEs at five slit widths. Data points below the dashed line indicate lower accuracy in NDEs compared with DEs. *Large dots*, mean thresholds; *small dots*, individual thresholds. (**C**) Mean slit width thresholds for NDEs and DEs. Mean thresholds of AEs and FEs are replotted for comparison. Error bars represent ±1 SEM.

(Figs. 2B, 2E). An AE/FE ratio of less than 1.0 indicates worse performance in AEs compared with FEs, reflecting temporal contour integration deficits in AEs. Significant interocular differences were observed at slit widths of 0.8, 1.0, 2.0, and 4.0 AIED for 1.5 cpd (*P*s < 0.05), but not at 0.4 AIED. For 3 cpd, significant differences were found at slit widths of 0.8 and 1.0 AIED (*P*s < 0.05) but not at 0.4, 2.0, or 4.0 AIED (*P*s > 0.05).

To further compare temporal contour integration abilities, we fitted psychometric functions using a Weibull function for each observer. The smooth curves in Figures 2A and 2D represent examples of the fitting for the mean data. From these fits, we estimated the slit width threshold at 75% accuracy for each observer (Figs. 2C, 2F). Amblyopic observers were stratified into three groups based on AE logMAR acuity before testing: mild (<0.3 logMAR), moderate (0.3 ≤ AE acuity ≤ 0.6 logMAR), and severe (>0.6 logMAR). Data points below the diagonal line in Figures 2C and 2F indicate higher thresholds in AEs compared with FEs. Significant differences in slit width thresholds between AEs and FEs were observed for all observers (1.5 cpd: $t_{14} = 4.08$, $P = 0.001$, Cohen's $d = 1.05$; 3 cpd: $t_{12} = 4.13$, $P = 0.001$, Cohen's $d = 1.15$; paired-sample t test). A trend toward higher AE slit width thresholds with worse AE visual acuity was evident. Specifically, 13 of 15 observers at 1.5 cpd and 11 of 13 observers at 3 cpd exhibited AE/FE ratios of greater than 1. The average AE/FE ratios of slit width thresholds for the three groups were consistent at more than 1 (mild amblyopia, 1.27 at 1.5 cpd; 1.15 at 3 cpd; moderate amblyopia, 1.44 at 1.5 cpd, 2.16 at 3 cpd; severe amblyopia, 1.50 at 1.5 cpd and 1.38 at 3 cpd). These results demonstrate significant temporal contour integration deficits in AEs, with the severity of deficits increasing with worse AE visual acuity.

Eleven visually normal children participated in experiment 1 as the control group and were only tested at a Gabor spatial frequency of 3 cpd (Fig. 3A). Psychometric functions for each observer in the control group were fitted using a Weibull function, with the smooth curves in Figure 3A representing examples of the fitting for the mean data. To assess interocular differences, five one-sample t tests were performed to analyze the accuracy ratio between the nondominant eye and dominant eye. No significant difference from 1.0 was found at any slit width (*P*s > 0.05) (Fig. 3B), confirming the absence of interocular differences in the control group. Consequently, the thresholds for the nondominant eye and dominant eye were averaged to represent the thresholds for normal control eyes (Fig. 3C). A one-way ANOVA with eye (AEs vs. normal control eyes) as a between-subject factor revealed a significant difference between AEs and normal control eyes, $F(1, 22) = 7.12$, $P = 0.01$, $\eta_p^2 = 0.25$. In contrast, the same analysis comparing FEs and normal control eyes showed no significant difference in thresholds ($P = 0.37$). These findings demonstrate temporal contour integration deficits in AEs compared with normal control eyes, whereas no such deficits were observed in the FEs of amblyopic children.

Relationships Between Temporal Contour Integration Deficits and Spatial Vision

To assess the potential influence of visual functions on temporal contour integration deficits in amblyopic children, we conducted Pearson's r correlation analyses. Amblyopic children were stratified into three groups based on their AE logMAR acuity: mild, moderate, and severe, as illustrated in Figure 4. The AE/FE ratio of slit width thresholds was not significantly correlated with the interocular difference in visual acuity at either spatial frequency: 1.5 cpd ($r = 0.51$; $P = 0.052$) (Fig. 4A) and 3 cpd ($r = 0.25$; $P = 0.41$) (Fig. 4D). Similarly, no significant correlation was observed between the AE/FE ratio of slit width thresholds and stereoacuity at 1.5 cpd ($r = 0.39$; $P = 0.15$) (Fig. 4B) or 3 cpd ($r = 0.16$; $P = 0.61$) (Fig. 4E). To explore the relationship between temporal and spatial contour integration deficits, we analyzed the correlation between the AE/FE ratio of slit width thresholds and the AE/FE ratio of static screen thresholds (no slit condition). No significant correlation was observed at either spatial frequency: 1.5 cpd ($r = -0.23$; $P = 0.42$) (Fig. 4C) or 3 cpd ($r = -0.24$; $P = 0.44$) (Fig. 4F). In summary, although the temporal contour integration deficits were evident in

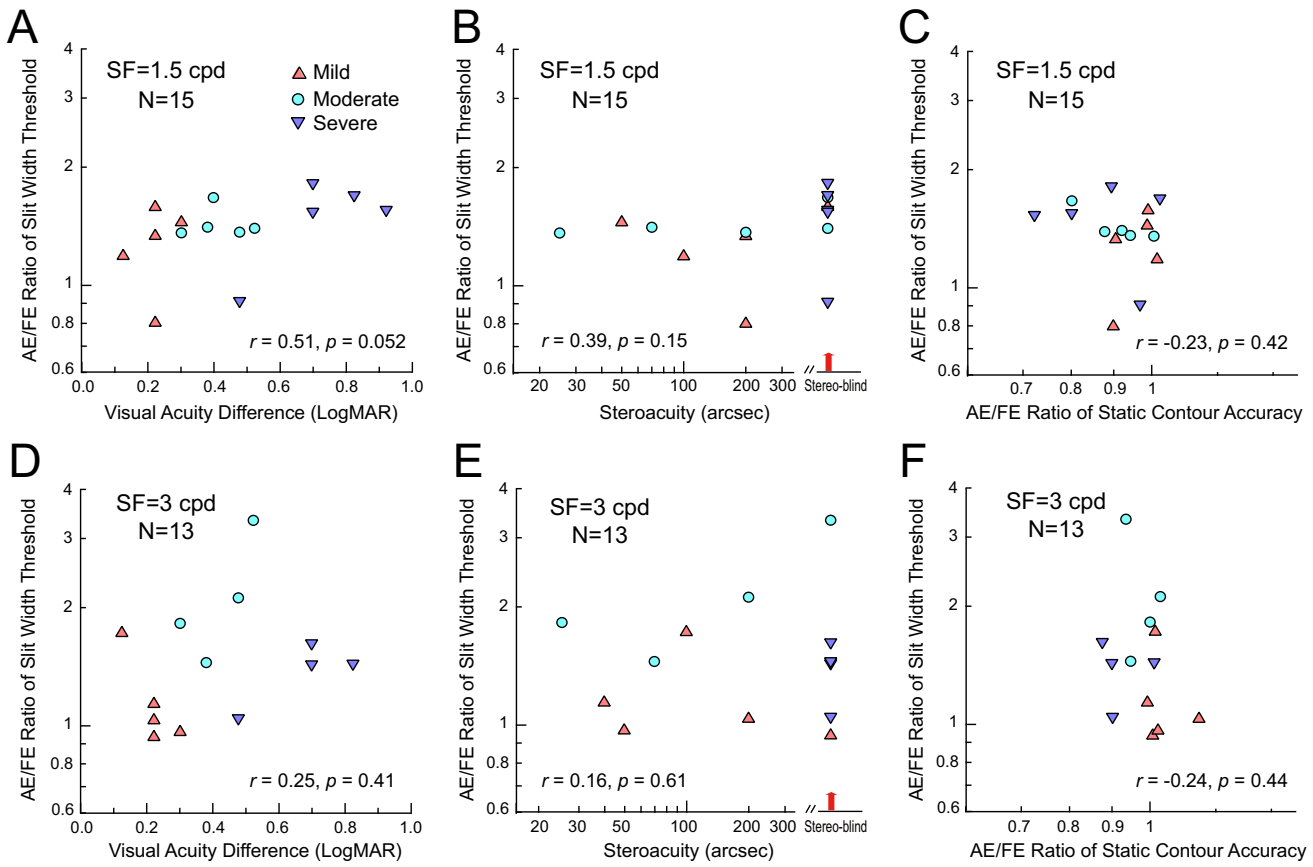

Figure 4. Relationship between temporal contour integration deficits and visual functions, as well as spatial contour integration deficits. (**A** and **D**) Visual acuity difference between AEs and FEs as a function of the AE/FE ratio of slit width thresholds at 1.5 cpd (**A**) and 3 cpd (**D**). (**B** and **E**) Stereoacuity as a function of the AE/FE ratio of slit width thresholds at 1.5 cpd (**B**) and 3 cpd (**E**). *Arrows* on the *x* axis indicate amblyopic observers who failed the Randot Stereo Test (stereo blind). For analysis purposes, their stereoacuity was set at 500 arcsec, a value below the lowest measurable score. (**C** and **F**) AE/FE ratio of static screen thresholds as a function of the AE/FE ratio of slit width thresholds at 1.5 cpd (**C**) and 3 cpd (**F**). Each symbol represents data for an individual observer: *triangles*, mild amblyopia; *circles*, moderate amblyopia; *inverted triangles*, severe amblyopia.

amblyopic children, these deficits were not significantly correlated with interocular acuity differences, stereoacuity, or spatial contour integration deficits.

The Effect of Gabor Orientation Collinearity in Temporal Contour Integration in Amblyopic Children

Previous studies on spatial contour integration have established that regularities such as collinearity and co-circularity, which align with the Gestalt grouping rule of good continuity, occur frequently in natural scenes.[28,71] In experiment 2, we examined whether collinearity is also critical for temporal contour integration. Fifteen amblyopic observers (13 from experiment 1) performed the contour detection task under five Gabor orientation jitter conditions (within 0°, ±10°, ±20°, ±30° or ±45° jitter from the contour path). The slit width was fixed at 1 AIED, and the stimulus moved at a speed of 6.4°/s. Gabor spatial frequencies of 1.5 and 3 cpd were tested. Ten visually normal children participated as the control group, tested only at 3 cpd.

The mean accuracy for each group is shown in Figures 5A and 5C. Detection accuracy decreased as orientation jitter increased, with performance barely above chance level at ±45° jitter, where collinearity was strongly disrupted. A three-way ANOVA with Gabor spatial frequency (1.5 and 3 cpd), eye (AEs vs. FEs), and orientation jitter (0°, ±10°, ±20°, ±30°, and ±45°) as repeated measure revealed significant main effects of eye, $F(1, 13) = 14.10$, $P = 0.002$, $\eta_p^2 = 0.52$, and orientation jitter, $F(4, 52) = 36.41$, $P < 0.001$, $\eta_p^2 = 0.74$, indicating significant detection differences between AEs and FEs. Further one-sample *t* tests on the AE/FE accuracy ratio (Figs. 5B, 5D) showed significant interocular differences only at 0° orientation jitter (1.5 cpd: AE/FE ratio = 0.94, $t_{14} = -2.77$, $P = 0.015$, Cohen's $d = -0.72$; 3 cpd: AE/FE ratio = 0.94, $t_{13} = -2.49$, $P = 0.027$, Cohen's $d = -0.67$). No significant differences were observed at other jitter conditions (*P*s > 0.05).

To compare AEs and normal control eyes, a one-way ANOVA with orientation jitter as repeated measure and group (amblyopic vs. control) as a between-subject factor revealed a significant main effect of the group, $F(1, 22) = 8.02$, $P = 0.01$, $\eta_p^2 = 0.27$, and a significant interaction between orientation jitter and group, $F(4, 88) = 7.50$, $p < 0.001$, $\eta_p^2 = 0.25$. Pairwise comparisons indicated that this interaction was primarily driven by significant differences between AEs and normal control eyes at 0° and ±10° jitter

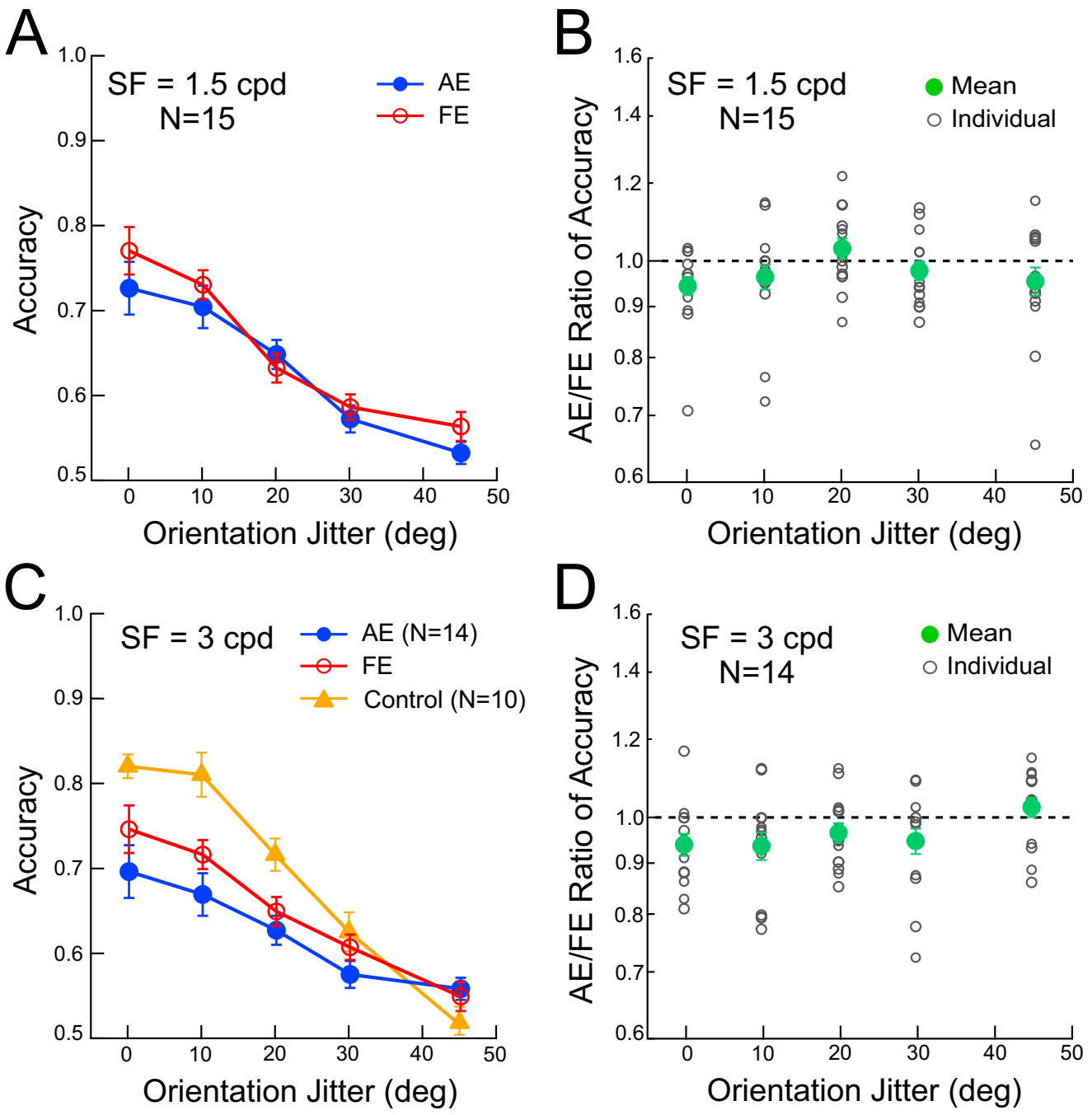

Figure 5. Effects of Gabor orientation jitter on temporal contour integration. (**A** and **C**) Mean accuracy of AEs, FEs, and normal control eyes as a function of the orientation jitter of individual contour elements from the contour path at 1.5 cpd (**A**) and 3 cpd (**C**). (**B** and **D**) AE/FE ratio of accuracy as a function of the orientation jitter of individual contour elements from the contour path at 1.5 cpd (**B**) and 3 cpd (**D**). *Large dots*, mean thresholds; *small dots*, individual thresholds. Error bars represent ±1 SEM.

(Ps < 0.05). A separate one-way ANOVA comparing FEs and normal control eyes showed no significant main effect of the group ($P = 0.08$), suggesting no performance difference between FEs and normal control eyes as a function of orientation jitter.

Our results demonstrate that Gabor orientation collinearity, when available, contributes to temporal contour integration in both amblyopic and normal vision. Amblyopic observers could detect temporal contours with complete orientation collinearity but exhibited deficits, whereas they failed to detect contours when collinearity was disrupted.

The Effect of Moving Speed in Temporal Contour Integration in Amblyopic Children

In experiment 3, we examined the dynamics of contour integration by investigating the effect of moving speed on temporal contour integration. Eight amblyopic observers

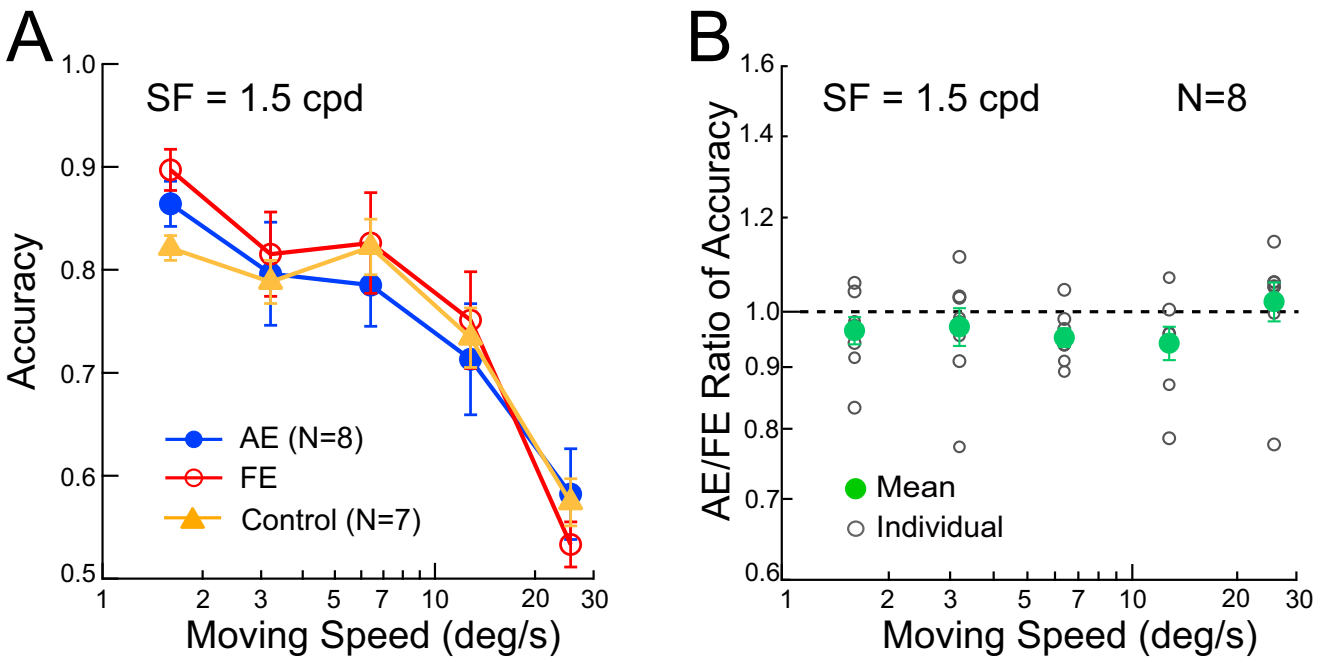

Figure 6. Effects of stimulus moving speed on temporal contour integration. (**A**) Mean accuracy of AEs, FEs, and normal control eyes as a function of stimulus moving speed. (**B**) AE/FE ratio of accuracy as a function of stimulus moving speed. Large dots: mean thresholds; small dots: individual thresholds. Error bars represent ±1 SEM.

(seven of whom also participated in experiments 1 and 2) performed the contour detection task under five moving speed conditions: 1.6°/s, 3.2°/s, 6.4°/s, 12.8°/s or 25.6°/s. The slit width was fixed at 1 AIED, and the Gabor spatial frequency was set at 1.5 cpd. Seven visually normal children participated as the control group.

The mean accuracy of contour detection for each group is shown in Figure 6A. A two-way ANOVA with the eye (AEs vs. FEs) and moving speed (1.6°/s, 3.2°/s, 6.4°/s, 12.8°/s, and 25.6°/s) as repeated measures revealed no significant main effect on the eye ($P = 0.24$) but a significant main effect of the moving speed, $F(4, 28) = 18.48$, $P < 0.001$, $\eta_p^2 = 0.73$, indicating a significant decline in performance of both AEs and FEs as the moving speed increased. At 25.6°/s, a speed too fast for contour identification, the accuracy of AEs, FEs, and normal control eyes was barely above chance level. A one-way ANOVA with moving speed as a repeated measure and group (amblyopic vs. control) as a between-subject factor showed no significant main effect of group ($P = 0.99$). Similarly, no significant difference in accuracy was observed between FEs and normal control eyes ($P = 0.57$).

To examine the interocular difference in moving speed for amblyopic children specifically, we conducted one-sample *t* tests on the AE/FE accuracy ratio (Fig. 6B). A significant interocular difference was found at 6.4°/s (AE/FE ratio = 0.96, $t_7 = -2.68$, $P = 0.031$, Cohen's $d = -0.95$), but not at other moving speeds (Ps > 0.05). These findings suggest that interocular differences in temporal contour integration for amblyopic children are present at moderate moving speeds but not at very slow or very fast speeds. Notably, seven observers who performed the contour detection task under the same condition three times (across experiments 1–3) showed no significant improvement in performance (mean improvement from test 1 to test 3 = −0.44% ± 2.96%).

Discussion

In this study, we investigated spatial–temporal visual integration in amblyopic children by exploring dynamic contour integration under a slit viewing condition. Our results showed significant temporal contour deficits in AEs compared with FEs, whereas no differences were found between FEs and normal control eyes. Notably, temporal contour integration deficits in AEs were most pronounced under conditions of complete collinearity and moderate stimulus moving speeds. Furthermore, the temporal contour integration ability between AEs and FEs, defined as the AE/FE ratio of slit width thresholds, was uncorrelated with interocular acuity differences, stereoacuity, and spatial contour integration deficits.

Our study demonstrates that amblyopia exhibits deficits in temporal contour processing. Specifically, AEs required larger slit widths to achieve performance levels comparable to FEs, and children with worse AE visual acuity exhibited greater slit width requirements. These results align with prior studies documenting temporal deficits in amblyopic visual systems, including reduced temporal resolution,[25,72] degraded temporal contrast sensitivity,[11] increased temporal synchrony thresholds,[19,20] and an expanded temporal binding window.[73] Such spatiotemporal deficits may arise from delayed information processing in the AE,[74,75] as evidenced by reduced neural synchronization in the amblyopic visual cortex.[76] Additionally, these deficits likely reflect reduced processing efficiency in the amblyopic visual system, attributable partly to reduced template efficiency but, to a greater extent, to a higher fraction of internal noise.[15,26,77]

The lack of correlation between the AE/FE ratio of slit width thresholds and interocular acuity differences, stereoacuity, or spatial contour integration deficits supports

Investigative Ophthalmology & Visual Science

the hypothesis that temporal deficits in amblyopia are independent of spatial vision impairments.[16,19–21,25,26] For instance, Aaen-Stockdale and Hess[16] demonstrated that the global motion deficit in amblyopia persisted even after accounting for low-level processing impairments, suggesting that these deficits cannot be explained solely by local motion input. Similarly, contour integration is often more disrupted in amblyopia than predicted by acuity deficits alone.[57,58,60] For example, our recent work showed that children treated for anisometropic amblyopia retain contour integration deficits even after compensating for the low-level deficits.[60] Our results indicate that worse AE acuity correlates with larger slit widths for temporal contour integration, consistent with prior findings linking visual function deficits to AE acuity.[2] Although poor acuity in AEs likely contributes to slower processing and reduced temporal integration efficiency,[74,75] acuity deficits alone cannot fully explain the observed temporal contour integration deficits. By using 90% contrast Gabor elements at lower spatial frequencies (1.5 and 3 cpd), where amblyopic spatial deficits are minimal, we minimized the influence of acuity and contrast sensitivity loss, which primarily occurs at high spatial frequencies.[3] These results suggest that, in addition to low-level deficits, higher-level temporal processing mechanisms are impaired in amblyopia.

Our results also highlight the role of element orientation collinearity in temporal contour integration for both amblyopic and normal vision. This finding aligns with previous studies on spatial contour integration in individuals with normal vision and amblyopia[55,78] as well as temporal contour integration in normal adult vision.[64] Collinearity might help to reduce external noise by establishing a predictable spatial structure, enabling efficient spatiotemporal integration.[79] Although FEs outperformed AEs in using collinearity for temporal contour integration, this advantage diminished when collinearity was disrupted by elevated external noise. Although collinearity facilitates integration by reducing external noise, AEs are less effective than FEs in leveraging this benefit owing to significantly higher internal noise levels.[15,26,77] Consequently, the higher internal noise likely impairs the AE's ability to process and integrate collinear information effectively, leading to the observed deficits in temporal contour integration.

Lateral connections are widely regarded as a primary mechanism for integrating contour elements into spatially extended contours.[80] Strong parallels exist between the rules governing collinear facilitation and contour integration, because both processes depend critically on factors such as orientation, spacing, and spatial frequency.[81] Abnormal lateral interactions in amblyopia, including reduced collinear facilitation, impaired contour integration, and disrupted spatial summation,[50–54,82–84] may underlie the grouping deficits and perceptual distortions commonly observed in amblyopia. However, it remains unclear whether the same neural mechanisms are responsible for both contour integration and collinear facilitation.[43,85,86] Contour integration may additionally involve higher-level visual regions that integrate global shape information.[44–49] Further research is needed to elucidate the specific contributions of these mechanisms to visual processing deficits in amblyopia.

We found no significant difference in temporal contour integration performance between the FEs of amblyopic children and normal control eyes, although there is proof of the presence of temporal processing deficits in the FE.[14–16,19] For example, Hayward et al.[14] demonstrated that global motion thresholds were elevated in the FEs of amblyopic children, with deficit manifesting in a speed-dependent manner. Specifically, abnormal visual input during childhood adversely affected slow motion-defined form perception, but not fast motion-defined form perception. In our study, interocular differences between AEs and FEs in temporal contour integration were observed only at a moderate moving speed (6.4°/s), but not at slower or faster speeds. Previous studies have reported global motion processing deficits in amblyopia.[22,26,87] These studies suggest that two independent speed-tuned systems mediate fast and slow motion perception, in which the fast system becomes more active as speed increases until an upper limit of about 80°/s, while the slow system is active at speeds less than 3°/s.[88–90] The speed-tuned results may not be independent across tasks or limited to tasks involving noise.[22] These findings highlight the importance of using carefully designed stimuli with appropriate sensitivity to evaluate global motion function in the clinical population.

Neuroimaging studies suggest that the temporal integration of successive visual information during slit viewing involves a distributed cortical network, including higher visual areas and parietal association areas.[91–93] Although early ventral visual areas are found to play an important role in spatial contour integration,[44] temporal contour integration under slit viewing conditions primarily engages higher dorsal visual areas such as V3B and MT, higher ventral visual areas like lateral occipital complex that are responsible for shape processing, and the posterior parietal cortex that is involved in visual memory.[64] Under the slit viewing conditions, especially at slit widths smaller than 1 AIED (where no more than two neighboring contour elements are visible simultaneously), the role of long-range horizontal interactions between V1 neurons is minimized. We speculated that deficits in temporal contour integration likely reflect abnormalities in the extrastriate cortex caused by amblyopia, consistent with prior reports of extrastriate network deficits in amblyopia.[94–96]

Although our study provides valuable insights into temporal contour integration in amblyopic children, it has several limitations that warrant consideration. First, our findings are based primarily on anisometropic amblyopes. The patterns of visual loss might differ between strabismic and anisometropic amblyopia.[1] Future studies should include other types of amblyopia for a more comprehensive understanding. Second, the average age of amblyopic children and children with normal vision is approximately 11 years. Although evidence suggests that visual temporal integration windows are adult-like in 5- to 7-year-old children,[97] future studies should include observers from different age groups to better understand the developmental characteristics of temporal contour processing. Third, we did not explore the potential for recovery of temporal processing in older amblyopic children, although perceptual learning has shown promise in improving visual function in amblyopia, particularly in spatial vision.[98,99] Further research is needed to develop targeted rehabilitation methods for temporal processing deficits in amblyopia.

Acknowledgments

Supported by the Natural Science Foundation of China grant 32371079 (JYZ; Beijing, China). The authors thank Dennis Levi, Lei Liu, Cong Yu, and Shu-Guang Kuai for their insightful comments and discussions. We also sincerely thank the partici-

pating children and their parents for their contributions to this study.

Disclosure: **Y.-R. Chen**, None; **S.-Q. Jiang**, None; **X.-Y. Liu**, None; **J.-Y. Zhang**, None

References

1. Kiorpes L, Daw N. Cortical correlates of amblyopia. *Vis Neurosci*. 2018;35:E016.
2. Levi DM, Mckee SP, Movshon JA. Visual deficits in anisometropia. *Vis Res*. 2011;51:48–57.
3. Levi DM, Harwerth RS. Spatio-temporal interactions in anisometropic and strabismic amblyopia. *Invest Ophthalmol Vis Sci*. 1977;16:90–95.
4. Bradley A, Freeman RD. Contrast sensitivity in anisometropic amblyopia. *Invest Ophthalmol Vis Sci*. 1981;21:467–476.
5. Giaschi D, Lo R, Narasimhan S, Lyons C, Wilcox LM. Sparing of coarse stereopsis in stereodeficient children with a history of amblyopia. *J Vision*. 2013;13:17.
6. McKee SP, Levi DM, Movshon JA. The pattern of visual deficits in amblyopia. *J Vision*. 2003;3:380–405.
7. Hess RF, Wang YZ, Demanins R, Wilkinson F, Wilson HR. A deficit in strabismic amblyopia for global shape detection. *Vision Res*. 1999;39:901–14.
8. Dallala R, Wang YZ, Hess RF. The global shape detection deficit in strabismic amblyopia: contribution of local orientation and position. *Vis Res*. 2010;50:1612–1617.
9. Birch EE, Kelly KR, Giaschi DE. Fellow eye deficits in amblyopia. *J Binocul Vis Ocul Motil*, 2019;69:116–125.
10. Meier K, Giaschi D. Unilateral amblyopia affects two eyes: fellow eye deficits in amblyopia. *Invest Ophthalmol Vis Sci,* 2017;58:1779–1800.
11. Kosovicheva A, Ferreira A, Vera-Diaz FA, Bex PJ. Effects of temporal frequency on binocular deficits in amblyopia. *Vis Res*. 2019;163:52–62.
12. Manny RE, Levi DM. Psychophysical investigations of the temporal-modulation sensitivity function in amblyopia - spatiotemporal interactions. *Invest Ophthalmol Vis Sci*. 1982;22:525–534.
13. Wang J, Ho CS, Giaschi DE. Deficient motion-defined and texture-defined figure-ground segregation in amblyopic children. *J Pediatr Ophthalmol Strabismus*. 2007;44:363–371.
14. Hayward J, Truong G, Partanen M, Giaschi D. Effects of speed, age, and amblyopia on the perception of motion-defined form. *Vis Res*. 2011;51:2216–2223.
15. Simmers AJ, Ledgeway T, Hess RF, McGraw PV. Deficits to global motion processing in human amblyopia. *Vis Res*. 2003;43:729–738.
16. Aaen-Stockdale C, Hess RF. The amblyopic deficit for global motion is spatial scale invariant. *Vis Res*. 2008;48:1965–1971.
17. Sireteanu R, Bäumer CC, Iftime A. Temporal instability in amblyopic vision: relationship to a displacement map of visual space. *Invest Ophthalmol Vis Sci*. 2008;49:3940–3954.
18. Thiel A, Iftime A. Temporal instabilities in amblyopic perception: a quantitative approach. *Perception*, 2016;45:443–465.
19. Huang PC, Li JR, Deng DM, Yu MB, Hess RF. Temporal synchrony deficits in amblyopia. *Invest Ophthalmol Vis Sci*. 2012;53:8325–8332.
20. Tao CW, Wu YD, Gong L, et al. Abnormal monocular and dichoptic temporal synchrony in adults with amblyopia. *Invest Ophthalmol Vis Sci*. 2019;60:4858–4864.
21. Ho CS, Giaschi DE, Boden C, Dougherty R, Cline R, Lyons C. Deficient motion perception in the fellow eye of amblyopic children. *Vis Res*. 2005;45:1615–1627.
22. Giaschi DE, Regan D, Kraft SP, Hong XH. Defective processing of motion-defined form in the fellow eye of patients with unilateral amblyopia. *Invest Ophthalmol Vis Sci*. 1992;33:2483–2489.
23. Bonneh YS, Sagi D, Polat U. Spatial and temporal crowding in amblyopia. *Vis Res*. 2007;47:1950–1962.
24. Tang Y, Chen LY, Liu ZJ, Liu CY, Zhou YF. Low-level processing deficits underlying poor contrast sensitivity for moving plaids in anisometropic amblyopia. *Vis Neurosci*. 2012;29:315–323.
25. Hu X, Qin Y, Ying XX, et al. Temporal characteristics of visual processing in amblyopia. *Front Neurosci*. 2021;15:3673491.
26. Kiorpes L, Tang C, Movshon JA. Sensitivity to visual motion in amblyopic macaque monkeys. *Vis Neurosci*. 2006;23:247–256.
27. Hamm LM, Black J, Dai SA, Thompson B. Global processing in amblyopia: a review. *Front Psychol*. 2014;5:583.
28. Field DJ, Hayes A, Hess RF. Contour integration by the human visual system: evidence for a local "association field". *Vision Res*. 1993;33:173–193.
29. Polat U, Sagi D. Lateral interactions between spatial channels - suppression and facilitation revealed by lateral masking experiments. *Vis Res*. 1993;33:993–999.
30. Polat U, Sagi D. The architecture of perceptual spatial interactions. *Vis Res*. 1994;34:73–78.
31. Polat U, Sagi D. Spatial interactions in human vision - from near to far via experience-dependent cascades of connections. *Proc Natl Acad Sci USA*. 1994;91:1206–1209.
32. Li ZP. A neural model of contour integration in the primary visual cortex. *Neural Comput*. 1998;10:903–940.
33. Ullman S, Gregory RL, Atkinson J. Low-level aspects of segmentation and recognition. *Phil Trans R Soc London B Biol Sci*. 1992;337:371–379.
34. VanRullen R, Delorme A, Thorpe SJ. Feed-forward contour integration in primary visual cortex based on asynchronous spike propagation. *Neurocomputing*. 2001;38:1003–1009.
35. Pettet MW, Mckee SP, Grzywacz NM. Constraints on long range interactions mediating contour detection. *Vis Res*. 1998;38:865–879.
36. Yen SC, Finkel LH. Extraction of perceptually salient contours by striate cortical networks. *Vis Res*. 1998;38:719–741.
37. Kapadia MK, Westheimer G, Gilbert CD. Spatial distribution of contextual interactions in primary visual cortex and in visual perception. *J Neurophysiol*. 2000;84:2048–2062.
38. Li W, Piech V, Gilbert CD. Contour saliency in primary visual cortex. *Neuron*. 2006;50:951–62.
39. Kapadia MK, Ito M, Gilbert CD, Westheimer G. Improvement in visual sensitivity by changes in local context - parallel studies in human observers and in V1 of alert monkeys. *Neuron*. 1995;15:843–856.
40. Bauer R, Heinze S. Contour integration in striate cortex - classic cell responses or cooperative selection? *Exp Brain Res*. 2002;147:145–152.
41. Gilad A, Meirovithz E, Slovin H. Population responses to contour integration: early encoding of discrete elements and late perceptual grouping. *Neuron*. 2013;78:389–402.
42. Mizobe K, Polat U, Pettet MW, Kasamatsu T. Facilitation and suppression of single striate-cell activity by spatially discrete pattern stimuli presented beyond the receptive field. *Vis Neurosci*. 2001;18:377–391.
43. Li W, Gilbert CD. Global contour saliency and local colinear interactions. *J Neurophysiol*, 2002;88:2846–56.
44. Altmann CF, Bülthoff HH, Kourtzi Z. Perceptual Organization of Local Elements into Global Shapes in the Human Visual Cortex. *Curr Biol*. 2003;13:342–349.

Investigative Ophthalmology & Visual Science

45. Kourtzi Z, Tolias AS, Altmann CF, Augath M, Logothetis NK. Integration of local features into global shapes: monkey and human fMRI studies. *Neuron*. 2003;23:333–346.
46. Chen M, Yan Y, Gong X, Gilbert CD, Liang H, Li W. Incremental integration of global contours through interplay between visual cortical areas. *Neuron*. 2014;82:682–94.
47. Li Y, Wang YH, Li S. Recurrent processing of contour integration in the human visual cortex as revealed by fMRI-guided tms. *Cerebral Cortex*. 2019;29:17–26.
48. Liang HL, Gong XJ, Chen MG, Yan Y, Li W, Gilbert CD. Interactions between feedback and lateral connections in the primary visual cortex. *Proc Natl Acad Sci USA*. 2017;114:8637–8642.
49. Mijovic B, De Vos M, Vanderperren K, et al. The dynamics of contour integration: a simultaneous EEG-fMRI study. *Neuroimage,* 2014;88:10–21.
50. Polat U, Sagi D, Norcia AM. Abnormal long-range spatial interactions in amblyopia. *Vis Res*. 1997;37:737–744.
51. Bonneh YS, Sagi D, Polat U. Local and non-local deficits in amblyopia: acuity and spatial interactions. *Vis Res*. 2004;44:3099–3110.
52. Levi DM, Hariharan S, Klein SA. Suppressive and facilitatory spatial interactions in amblyopic vision. *Vis Res*. 2002;42:1379–1394.
53. Ellemberg D, Hess RF, Arsenault AS. Lateral interactions in amblyopia. *Vis Res*. 2002;42:2471–2478.
54. Polat U, Bonneh Y, Ma-Naim T, Belkin M, Sagi D. Spatial interactions in amblyopia: effects of stimulus parameters and amblyopia type. *Vis Res*. 2005;45:1471–1479.
55. Hess RF, McIlhagga W, Field DJ. Contour integration in strabismic amblyopia: the sufficiency of an explanation based on positional uncertainty. *Vis Res*. 1997;37:3145–3161.
56. Kovács I, Polat U, Pennefather PM, Chandna A, Norcia AM. A new test of contour integration deficits in patients with a history of disrupted binocular experience during visual development. *Vis Res*. 2000;40:1775–1783.
57. Levi DM, Yu C, Kuai SG, Rislove E. Global contour processing in amblyopia. *Vision Res*. 2007;47:512–524.
58. Kozma P, Kiorpes L. Contour integration in amblyopic monkeys. *Vis Neurosci*, 2003;20:577–88.
59. Chandna A, Pennefather PM, Kovacs I, Norcia AM. Contour integration deficits in anisometropic amblyopia. *Invest Ophthalmol Vis Sci*. 2001;42:875–878.
60. Jiang SQ, Chen YR, Liu XY, Zhang JY. Contour integration deficits at high spatial frequencies in children treated for anisometropic amblyopia. *Front Neurosci*. 2023;17: 1160853.
61. Kovacs I, Polat U, Norcia AM. Breakdown of binding mechanisms in amblyopia. *Invest Ophthalmol Vis Sci*. 1996;37:3078–3078.
62. Hess RF, Demanins R. Contour integration in anisometropic amblyopia. *Vis Res*. 1998;38:889–894.
63. Parks TE. Post-retinal visual storage. *Am J Psychol*. 1965;80:572–585.
64. Kuai SG, Li W, Yu C, Kourtzi Z. Contour integration over time: psychophysical and fMRI evidence. *Cerebral Cortex,* 2017;27:3042–3051.
65. Gilbert CD, Wiesel TN. Columnar specificity of intrinsic horizontal and corticocortical connections in cat visual-cortex. *J Neurosci*. 1989;9:2432–2442.
66. Elliott MC, Firth AY. The logMAR Kay picture test and the logMAR acuity test: a comparative study. *Eye,* 2009;23:85–88.
67. Pelli DG. The VideoToolbox software for visual psychophysics: transforming numbers into movies. *Spat Vis*. 1997;10:437–442.
68. Mou T. Logarithmic visual acuity chart and five-score recording. *Chinese J Ophthalmol*. 1966;13:96–106.
69. Wichmann FA, Hill NJ. The psychometric function: I. Fitting, sampling, and goodness of fit. *Percept Psychophys*. 2001;63:1293–1313.
70. Stewart CE, Fielder AR, Stephens DA, Moseley MJ, Cooperative M. Treatment of unilateral amblyopia: factors influencing visual outcome. *Invest Ophthalmol Vis Sci*. 2005;46:3152–3160.
71. Geisler WS, Perry JS, Super BJ, Gallogly DP. Edge co-occurrence in natural images predicts contour grouping performance. *Vis Res*. 2001;41:711–724.
72. Spang K, Fahle M. Impaired temporal, not just spatial, resolution in amblyopia. *Invest Ophthalmol Vis Sci*. 2009;50:5207–5212.
73. Narinesingh C, Goltz HC, Wong AMF. Temporal binding window of the sound-induced flash illusion in amblyopia. *Invest Ophthalmol Vis Sci*. 2017;58:1442–1448.
74. Hamasaki DI, Flynn JT. Amblyopic eyes have longer reaction-times. *Invest Ophthalmol Vis Sci*. 1981;21:846–853.
75. Levi DM, Harwerth RS, Manny RE. Suprathreshold spatial-frequency detection and binocular interaction in strabismic and anisometropic amblyopia. *Invest Ophthalmol Vis Sci*. 1979;18:714–725.
76. Roelfsema PR, Konig P, Engel AK, Sireteanu R, Singer W. Reduced synchronization in the visual-cortex of cats with strabismic amblyopia. *Eur J Neurosci*. 1994;6:1645–1655.
77. Levi DM, Klein SA. Noise provides some new signals about the spatial vision of amblyopes. *J Neurosci*. 2003;23:2522–2526.
78. Hadad B, Maurer D, Lewis TL. The effects of spatial proximity and collinearity on contour integration in adults and children. *Vision Res*. 2010;50:772–8.
79. Baldwin AS, Fu M, Farivar R, Hess RF. The equivalent internal orientation and position noise for contour integration. *Sci Rep*. 2017;7:13048.
80. Loffler G. Perception of contours and shapes: low and intermediate stage mechanisms. *Vis Res*. 2008;48:2106–2127.
81. Polat U, Bonneh Y. Collinear interactions and contour integration. *Spatial Vis*. 2000;13:393–401.
82. Hariharan S, Levi DM, Klein SA. "Crowding" in normal and amblyopic vision assessed with Gaussian and Gabor C's. *Vis Res*. 2005;45:617–633.
83. Wong EH, Levi DM, McGraw PV. Spatial interactions reveal inhibitory cortical networks in human amblyopia. *Vis Res*. 2005;45:2810–2819.
84. Levi DM, Carney T. The effect of flankers on three tasks in central, peripheral, and amblyopic vision. *J Vision*. 2011;11:10–10.
85. Ito M, Komatsu H. Representation of angles embedded within contour stimuli in area V2 of macaque monkeys. *J Neurosci*. 2004;24:3313–3324.
86. Williams CB, Hess RF. Relationship between facilitation at threshold and suprathreshold contour integration. *J Opt Soc Am A Optics Image Sci Vis*. 1998;15:2046–2051.
87. El-Shamayleh Y, Kiorpes L, Kohn A, Movshon JA. Visual motion processing by neurons in area MT of macaque monkeys with experimental amblyopia. *J Neurosci*. 2010;30:12198–12209.
88. Edwards M, Badcock DR, Smith AT. Independent speed-tuned global-motion systems. *Vis Res*. 1998;38:1573–1580.
89. Khuu SK, Badcock DR. Global speed processing: evidence for local averaging within, but not across two speed ranges. *Vis Res*. 2002;42:3031–3042.
90. van de Grind WA, van Hof P, van der Smagt MJ, Verstraten FAJ. Slow and fast visual motion channels have independent binocular-rivalry stages. *Proc R Soc B Biol Sci*. 2001;268:437–443.
91. Yin C, Shimojo S, Moore C, Engel SA. Dynamic shape integration in extrastriate cortex. *Curr Biol*. 2002;12:1379–1385.

Investigative Ophthalmology & Visual Science

92. Bognár A, Vogels R. Moving a shape behind a slit: partial shape representations in inferior temporal cortex. *J Neurosci*. 2021;41:6484–6501.
93. Orlov T, Zohary E. Object representations in human visual cortex formed through temporal integration of dynamic partial shape views. *J Neurosci*. 2018;38:659–678.
94. Thompson B, Villeneuve MY, Casanova C, Hess RF. Abnormal cortical processing of pattern motion in amblyopia: evidence from fMRI. *Neuroimage*. 2012;60:1307–1315.
95. Lerner Y, Pianka P, Azmon B, et al. Area-specific amblyopic occipitotemporal object effects in human representations. *Neuron*. 2003;40:1023–1029.
96. Ho CS, Giaschi DE. Low- and high-level motion perception deficits in anisometropic and strabismic amblyopia: evidence from fMRI. *Vis Res*. 2009;49:2891–2901.
97. Freschl J, Melcher D, Kaldy Z, Blaser E. Visual temporal integration windows are adult-like in 5-to 7-year-old children. *J Vision*. 2019;19:5.
98. Liu XY, Zhang T, Jia YL, Wang NL, Yu C. The therapeutic impact of perceptual learning on juvenile amblyopia with or without previous patching treatment. *Invest Ophthalmol Vis Sci*. 2011;52:1531–1538.
99. Liu XY, Zhang YW, Gao F, Chen F, Zhang JY. Dichoptic perceptual training in children with amblyopia with or without patching history. *Invest Ophthalmol Vis Sci*. 2021;62:4.

Investigative Ophthalmology & Visual Science